Electronic Supplementary Material (ESI) for ChemComm.

Supporting information

Hydroxylation boosted low-overpotential CO2 reduction to ethylene for Cu/PTFE electrode

Yifeng Wang[a,b], Haoliang Huang[a,c], Shengjie Zhang[a], Hao Zhang[a], Chao Jing*[a,b], Jian-Qiang Wang*[a,b], Linjuan Zhang*[a,b]

[a]Key Laboratory of Interfacial Physics and Technology, Shanghai Institute of Applied Physics, Chinese Academy of Sciences, Shanghai 201800, P.R. China.
[b]University of Chinese Academy of Sciences, Beijing 100049, P.R. China.
[c]Songshan Lake Materials Laboratory, Dongguan 523808, P. R. China.

Materials

Carbon dioxide (CO_2, 99.999%) and Argon (Ar, 99.999%) were from Xiangkun Specialty Gases Co., Ltd. (Shanghai, China). Milli-Q water (18.2 MΩ cm) produced using the Milli-Q apparatus from Millipore (USA). Cu nanoparticles (Cu NPs, 10-30 nm particle size) was purchased from Macklin. Cu target (99.999%) was from Fuzhou Innovation Photoelectric Technology Co., Ltd. Carbon paper (GDL, YLS-30T) and Nafion solution (5 wt %) were from Sinero. Anion-exchange membrane (FAA-3-PK-130) was from shanghai chuxi industrial co. ltd. Polylactide (PLA) was from Caigle Technology Co., Ltd. Polytetrafluoroethylene (PTFE) membrane was from Beijing Zhongxingweiye Instrument Co., Ltd.

Electrode preparation

Cu-sputtered PTFE was prepared via ion sputtering on a sputter coater (108 Manual) at a current of 30 mA under vacuum at 0.06 mbar for 9 mins totally. M_Cu and D_Cu were sputtered in moist and dry argon atmosphere, respectively. M_Cu and D_Cu were directly used as electrode.

An ink containing a mixture of Nafion, isopropanol and Cu NPs was airbrushed (using N_2 gas as a carrier gas) on a carbon paper serving as substrate. After drying under vacuum, a round electrode with a diameter of about 1.6 cm was cut and assembled into a flow cell.

Characterization

The Cu-sputtered PTFE electrodes were characterized using SEM on a Zeiss Crossbeam 540 apparatus and TEM on a JEM 2100F FEI Tecnai F20 apparatus. X-ray diffraction (XRD) was measured on a D8 Advance X-ray diffractometer equipped with graphite-monochromatized Cu Kα radiation. The oxidation state of Cu in the samples were studied by X-ray photoelectron spectroscopy (XPS) (ESCALAB Xi+). Fourier-transform infrared spectroscopy (ATR-FTIR) experiments were conducted on a Vertex 80 FTIR spectrometer with CaF_2 as the prismatic window at room temperature. Static contact angle is measured on a SDC 350KS contact angle meter. The binding energy data were calibrated with reference to the C 1s signal at 284.8 eV. Raman spectral data were collected by using a confocal microscope (Horiba, LabRAM HR Evolution). The source of the excitation was a 473 nm laser beam. Calibration of spectra was carried out using a silicon wafer with a standard peak at 520.7 cm^{-1}. A three-electrode setup was used in the in situ Raman spectroscopy measurements in CO_2-saturated 0.5 M $KHCO_3$, including a working electrode of Au, a counter electrode made of platinum wire, and a Ag/AgCl reference electrode.

Electrochemical Measurements

Electrochemical measurements were performed in a flow cell configuration consisting of a gas diffusion layer, an anion exchange membrane and a nickel mesh anode, connected to a PGSTAT302N potentiostat (Metrohm Autolab, equipped with BA and FRA32M modules). The geometric active surface area of both anode and cathode are 1 cm^2. An Ag/AgCl electrode (with 3 M KCl as the filling solution) was used as the reference electrode. All the applied cathode potentials in the flow cell were converted to the reversible hydrogen electrode (RHE) reference scale with a standard compensation by:

$$E(V\ vs.\ RHE) = E(V\ vs.\ Ag/AgCl) + 0.197 + 0.059 \times pH - 90\% \times i \times R$$

Where R is the solution resistance, which was determined to be ca. 5 ω as shown in Fig. S10. A factor of 90% was applied for iR compensation during flow cell operation.

The gas products from CO_2RR were analyzed using a gas chromatograph (GC-2060) coupled with a thermal conductivity detector (TCD) and a flame ionization detector (FID).

Density functional theory calculation

In this work, the calculations were performed applying density functional theory (DFT) with the Perdew, Burke, and Ernzerhof generalized gradient functional (GGA-PBE)[1]using the Vienna Ab initio Simulation Package (VASP).[2, 3]Tkatchenko-Scheffler method[4]was used for van der Waals interactions correction. A 5 × 5 × 1 k-point mesh was used, with a 500 eV cutoff energy.

A four-layer FCC(111) model was used, with 3 × 3 unit cells consisting of 9 Cu atoms in each unit cell. The top two layers and the adsorbates were allowed to fully relax during relaxation calculations. A vacuum gap of approximately 15 Å was set along the surface normal direction. Nørskov's work[5] suggested that a charged water layer can significantly affect the intermediates' structures and energies. Therefore, extra water molecules and electric field were added during the calculations to better simulate the electrochemical environment. Based on Nørskov's calculations, the electric field was set to 0.9 V / Å along the z direction. To simulate the hydroxylation on copper surface, an extra OH was added on the surface, achieving an OH coverage θ ≈ 9.1%. The free energy G was calculated as:

G = E + ZPE -TS

where E is the electronic energy, ZPE is the zero-point energy, T is the temperature, and S is the entropy.

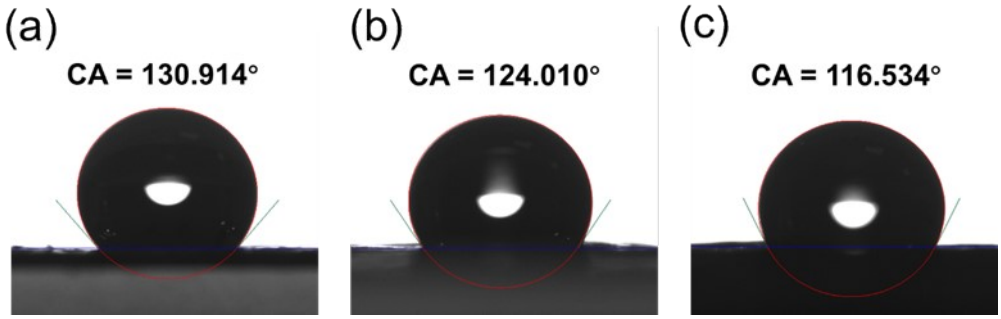

Fig. S1 Contact angel of (a) PTFE, (b) M_Cu and (c) Cu/carbon paper.

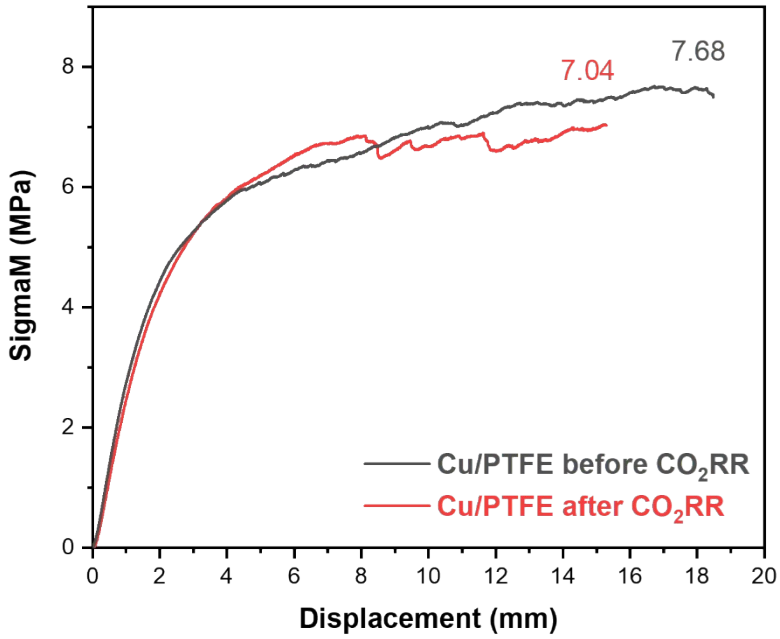

Fig. S2 Tensile strength measure of Cu/PTFE electrode before and after CO_2RR.

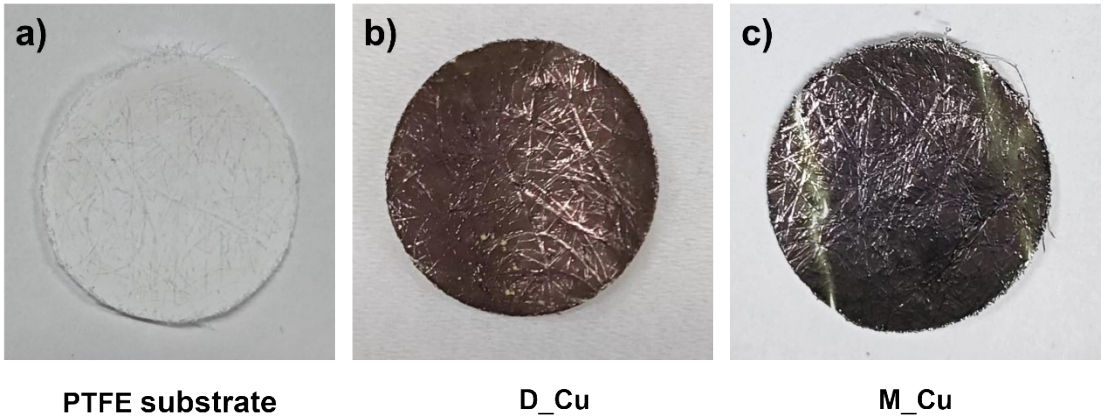

Fig. S3 Photograph of (a) PTFE substrate, (b) D_Cu, (c) M_Cu.

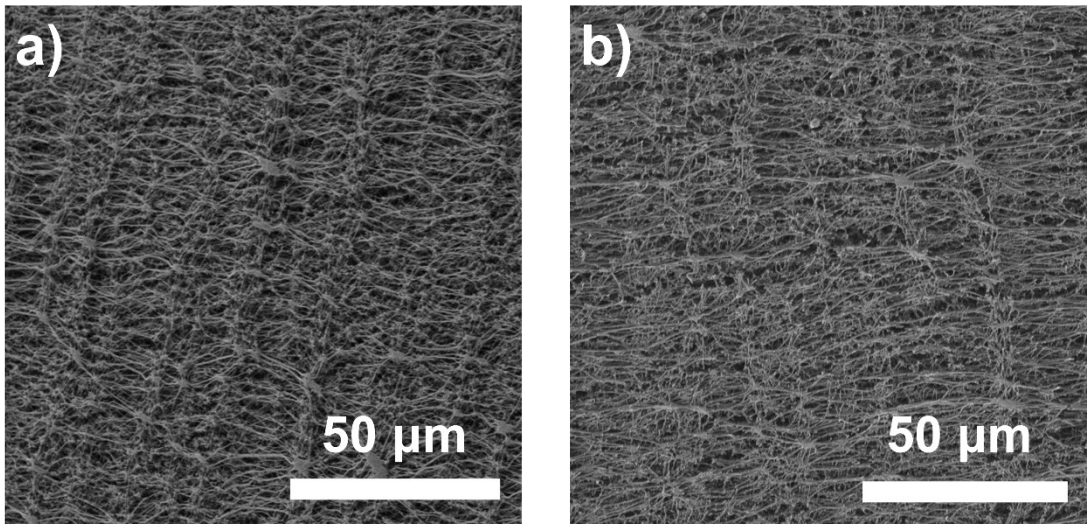

Fig. S4 SEM images of (a) blank PTFE membrane, (b) Cu-sputtered PTFE.

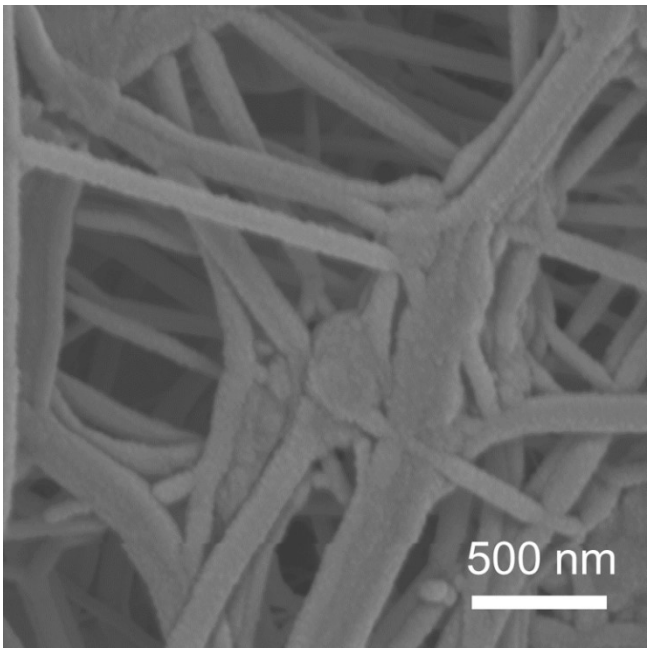

Fig. S5 SEM image of D_Cu.

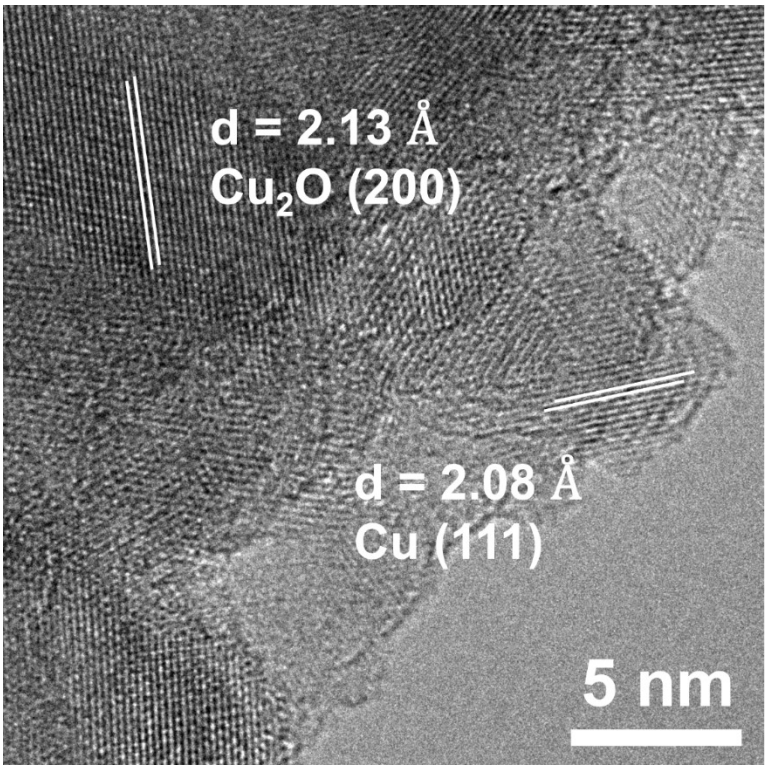

Fig. S6 TEM image of D_Cu.

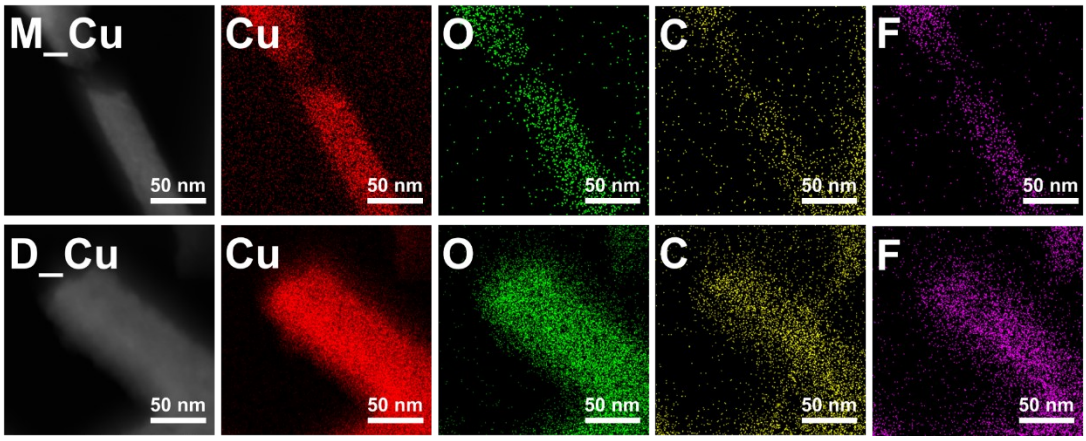

Fig. S7 TEM-EDS mapping of M_Cu (above) and D_Cu (below).

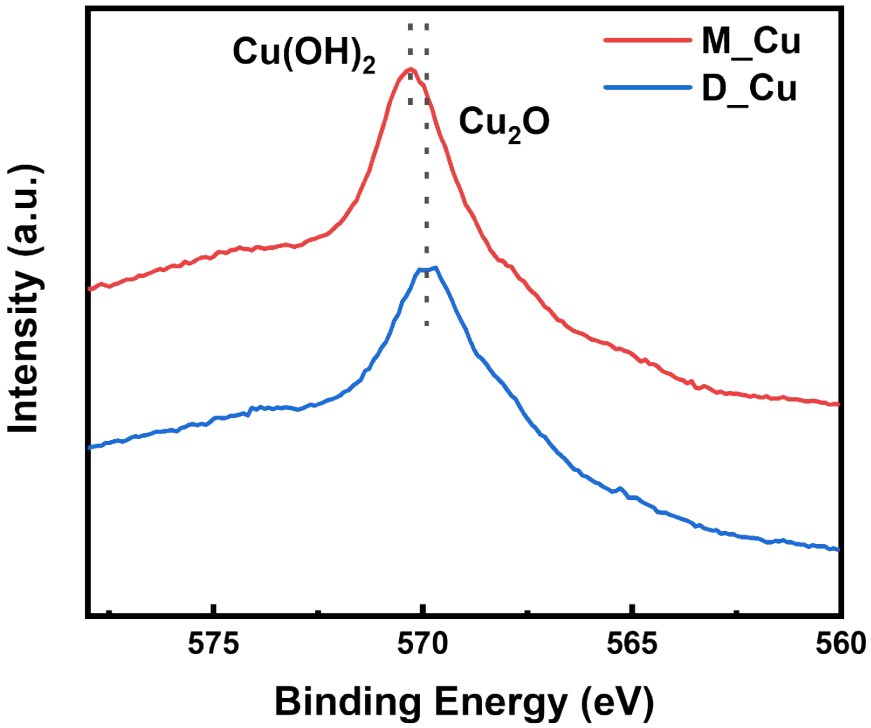

Fig. S8 Cu LMM of D_Cu and M_Cu.

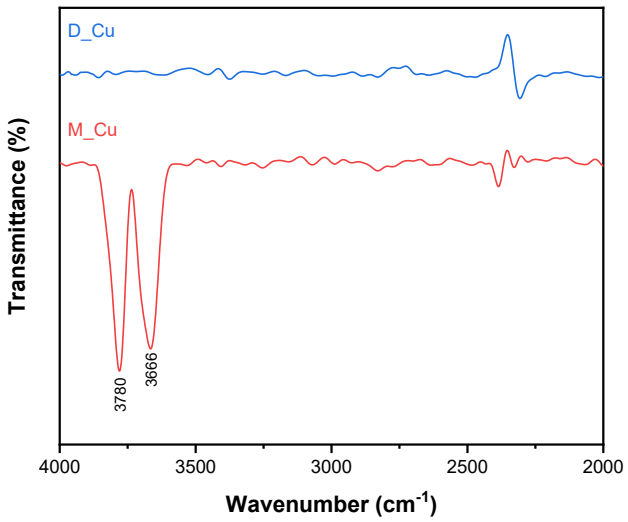

Fig. S9 Infrared spectra of M_Cu and D_Cu.

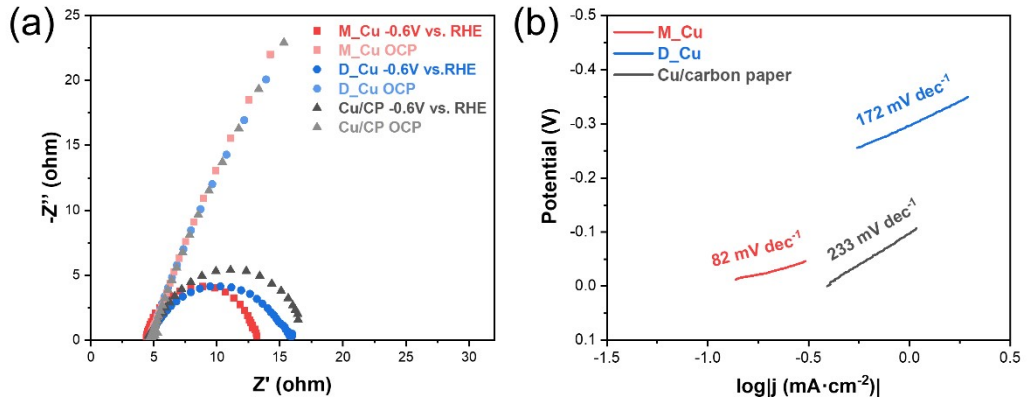

Fig. S10 (a) EIS of M_Cu, D_Cu and Cu/carbon paper at OCP and -0.6 V vs. RHE. (b) Tafel plots of M_Cu and D_Cu and Cu/carbon paper.

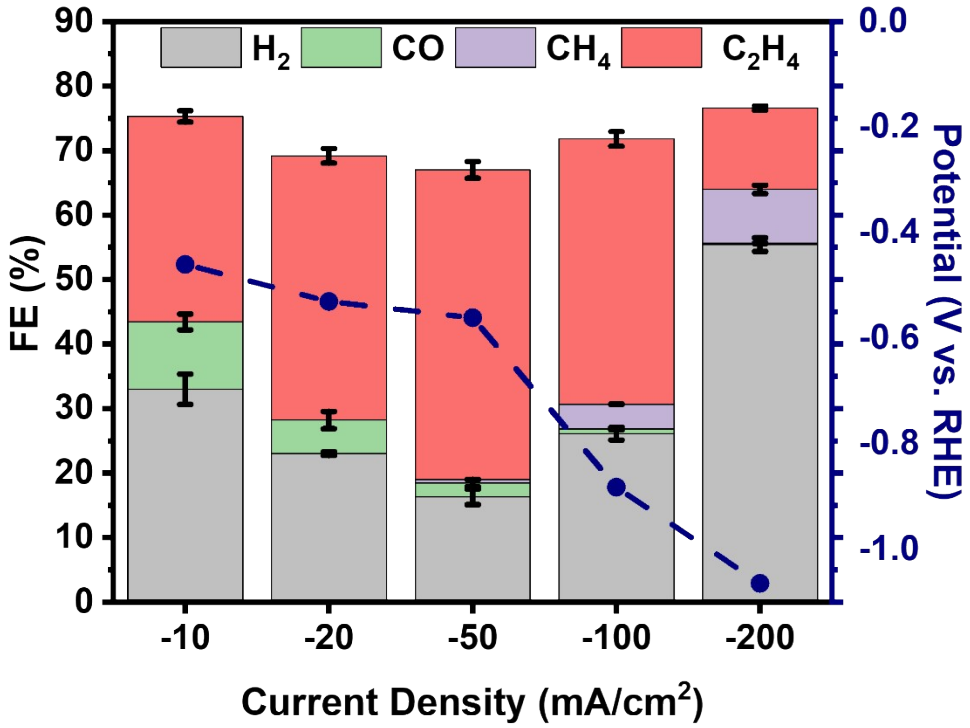

Fig. S11 Faradaic efficiency for each CO_2RR gaseous products of D_Cu at various current densities and corresponding potentials.

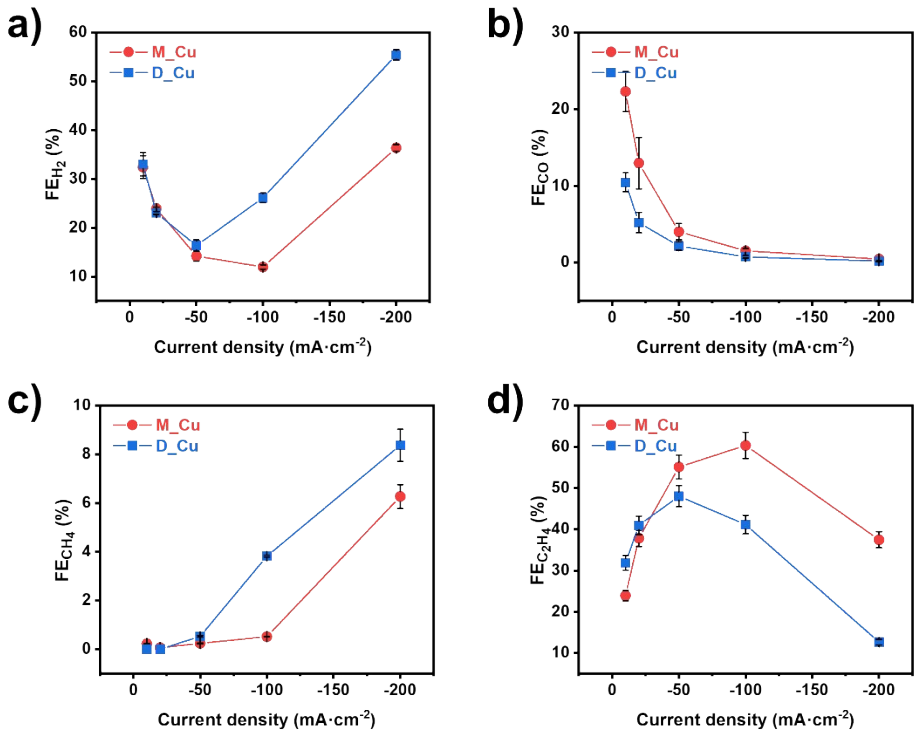

Fig. S12 Current density plotted against the FE for (a) H_2; (b) CO; (c) CH_4; (d) C_2H_4.

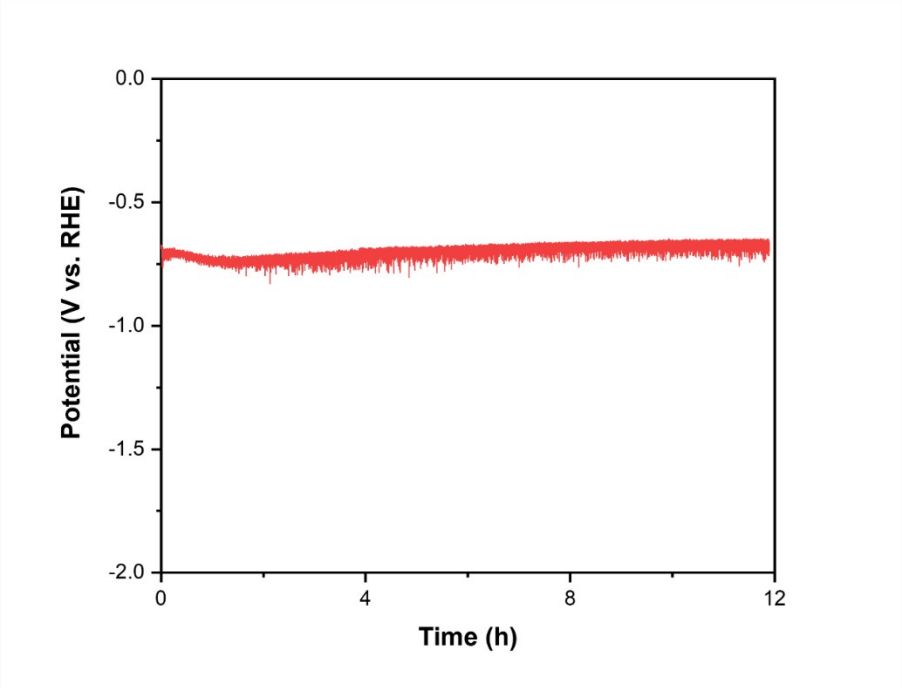

Fig. S13 CO_2RR stability measurement of M_Cu during 12h with an applied current density of -100 mA·cm^{-2}

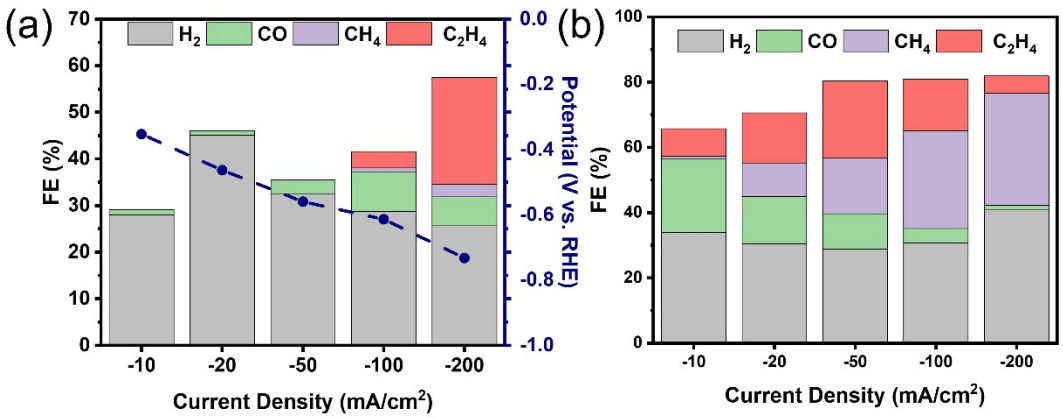

Fig. S14 (a) Faradaic efficiency for each CO_2RR gaseous products of commercial Cu nanoparticles (Cu NPs) at various current densities and corresponding potentials. (b) Faradaic efficiency for each CO_2RR gaseous products of copper sputtered carbon paper at various current densities

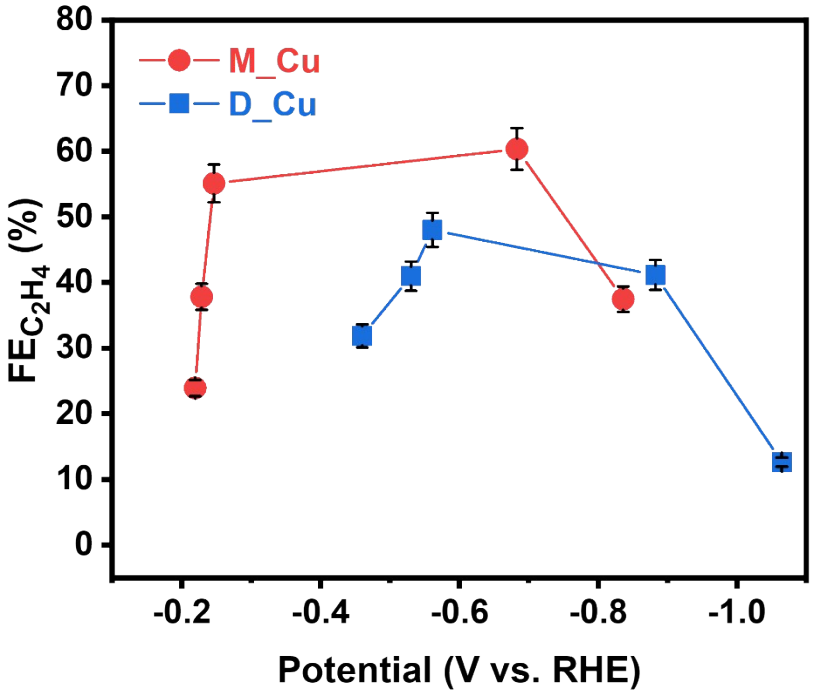

Fig. S15 Faradaic efficiency for C_2H_4 of M_Cu and D_Cu depending on the applied potentials.

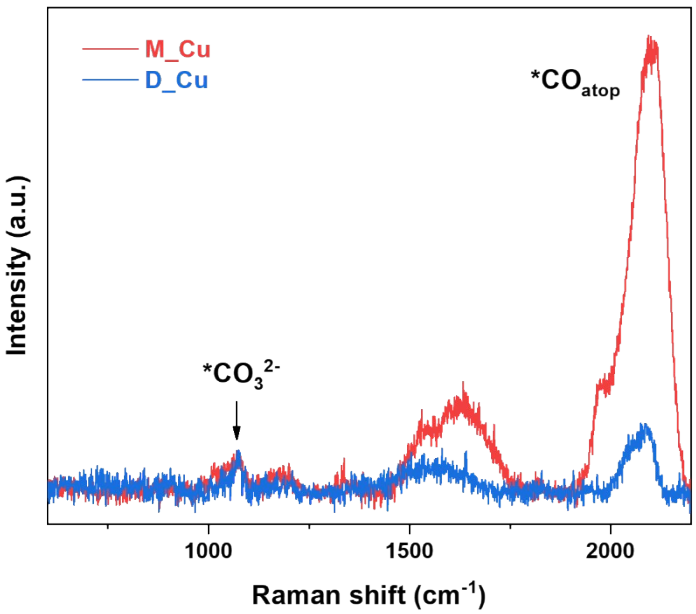

Fig. S16 Raman spectrum of M_Cu (0.2 V) and D_Cu (-0.1 V), normalized by the intensity of the *CO_3^{2-} peak.

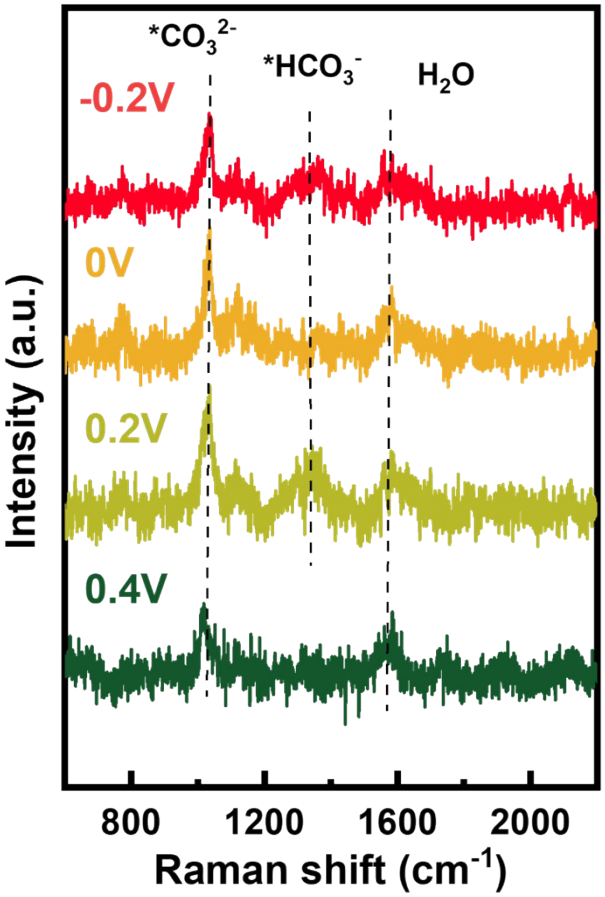

Fig. S17 In situ Raman of bare Au electrode.

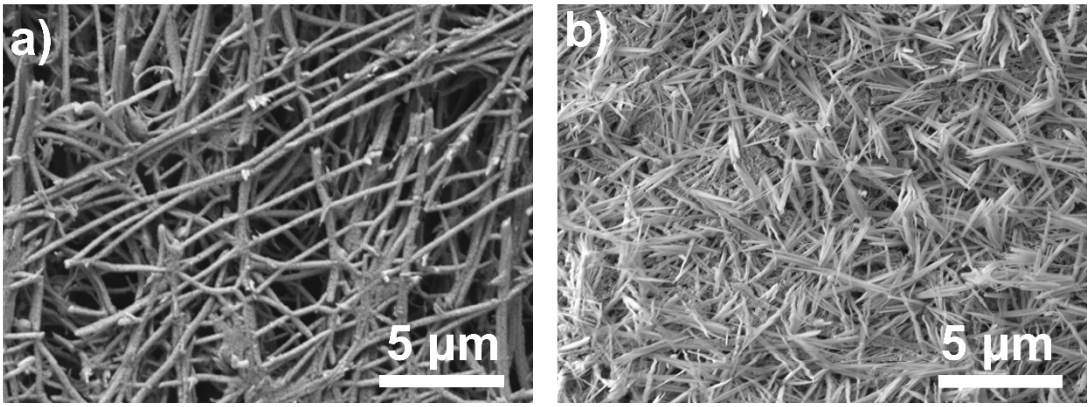

Fig. S18 SEM images of (a) post-reaction D_Cu. (b) post-reaction M_Cu.

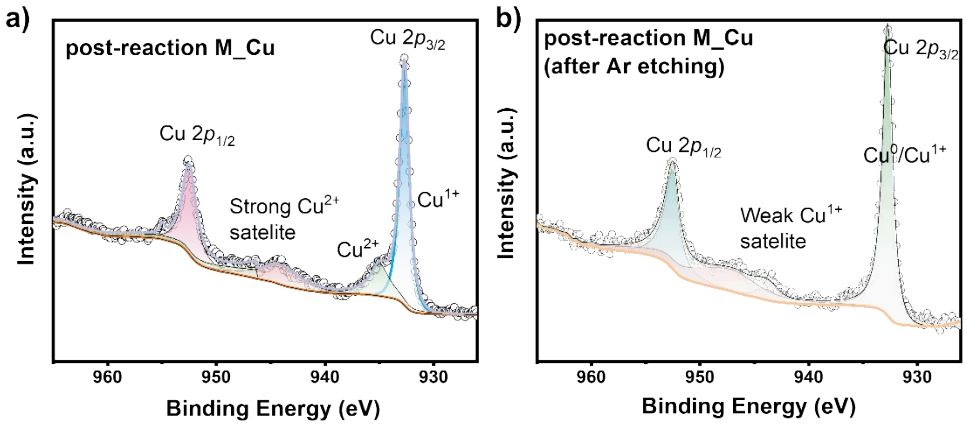

Fig. S19 XPS of (a) post-reaction M_Cu. (b) post-reaction M_Cu after Ar etching.

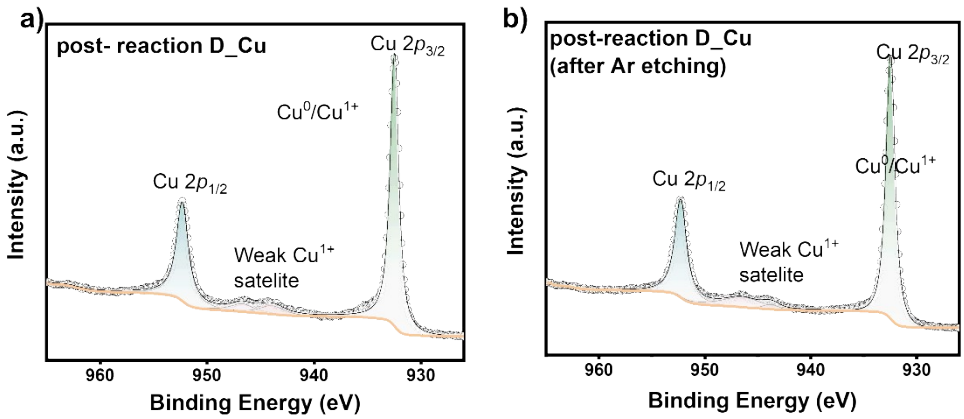

Fig. S20 XPS of (a) post-reaction D_Cu. (b) post-reaction D_Cu after Ar etching.

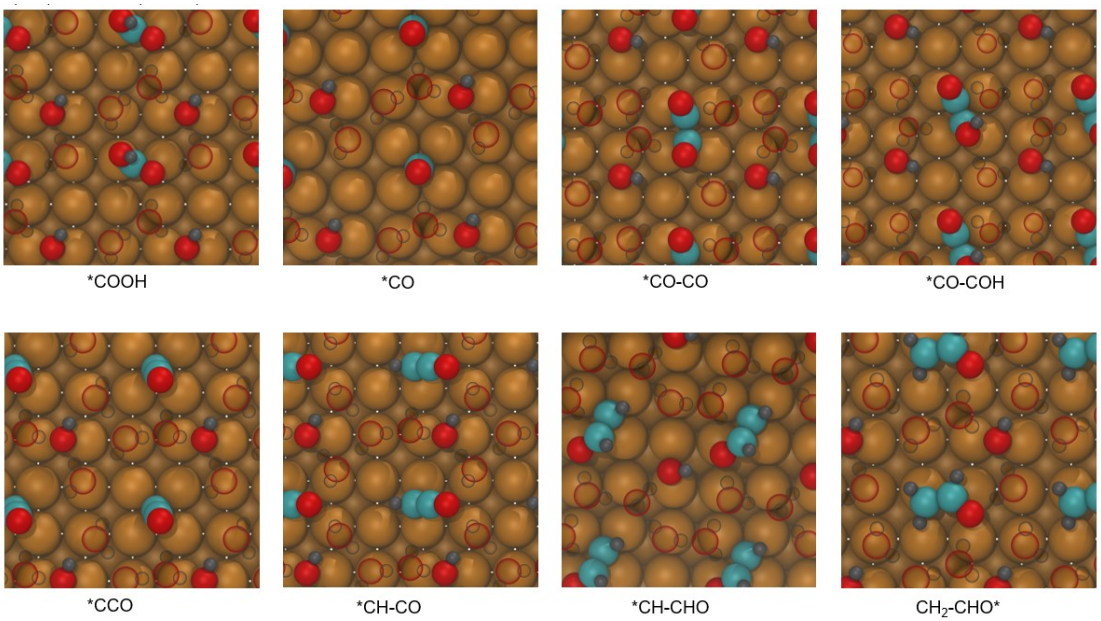

Fig. S21 DFT optimized intermediates of CO_2RR to C_2H_4 on Cu(111) surface. Cu: dark golden; C: cyan; O: red; H: gray.

references

1 J. P. Perdew, K. Burke and M. Ernzerhof, *Phys. Rev. Lett.*, 1996, **77**, 3865-3868.
2 G. Kresse and J. Furthmuller, *Comp. Mater. Sci.*, 1996, **6**, 15-50.
3 G. Kresse, *J Non-Cryst. Solids*, 1995, **193**, 222-229.
4 A. Tkatchenko and M. Scheffler, *Phys. Rev. Lett.*, 2009, **102**, 073005.
5 J. H. Montoya, C. Shi, K. Chan and J. K. Norskov, *J. Phys. Chem. Lett.*, 2015, **6**, 2032-2037.